Water Practice & Technology

IWA PUBLISHING

Water Practice & Technology Vol 17 No 5, 1019 doi: 10.2166/wpt.2022.036

Valorization of spent coffee grounds through pyrolysis as adsorbent for the removal of Vivizole Red 3BS dye from aqueous solution

Admasu Adamu [a,*], Feleke Zewge [a,b] and Yonas Chebude [a,b]

[a] Africa Center of Excellence for Water Management, Addis Ababa University, Addis Ababa, Ethiopia
[b] Department of Chemistry, College of Natural and Computational Sciences, Addis Ababa University, Addis Ababa, Ethiopia
*Corresponding author. E-mail: admasu.adamu@aau.edu.et

AA, 0000-0003-0296-9328

ABSTRACT

Ever-increasing coffee consumption results in the generation of a significant amount of solid residue in the form of spent coffee grounds (SCG) and their subsequent disposal causes environmental pollution. Valorization of SCG through pyrolysis could be one of the solutions to this challenge. Pristine biochar of SCG shows less efficiency to remove dyes from aqueous solutions. Herein, iron(III) salt was used as a catalyst during the carbonization of SCG and has a good graphitization efficiency and thus enhanced the formation of aromatic structures, which provide adsorption sites for the dye. The physical characteristics of the prepared biochar were analyzed by FTIR, XRD, and BET. A predictive model for the removal of the dye was investigated with the Design Expert 11.0 software through the central composite design (CCD) - response surface methodology (RSM) by conducting a batch adsorption study, and the suggested optimum values of the CCD were 10 ppm initial dye concentration, 1 g per 100 ml adsorbent dose, and contact time of 101 min with optimum predicted dye removal of 99%. The Langmuir model was the best fitted isotherm model with an adsorption capacity of 2.07 mg/g, and the adsorption kinetic equilibrium data was better described by the pseudo-second-order model and from the thermodynamic study, it has been suggested that the adsorption process was spontaneous, favorable, endothermic, and a physicochemisorption in nature. The possible adsorption mechanisms governing the adsorption process of the dye with biochar are $\pi - \pi$ electron donor-acceptor interactions and hydrogen bonding.

Key words: adsorption, biochar, pyrolysis, spent coffee ground, textile dye, valorization

HIGHLIGHTS

- Valorization of SCG waste through pyrolysis results in composite biochar.
- Iron(III) salt was used to catalyze the graphitization of biochar.
- Composite biochar helps to remove Vivizole Red 3BS dye from aqueous solution.
- Use of composite biochar as adsorbent offers an opportunity to manage the environmental impacts of SCG waste.
- The exhausted composite biochar is easily separated by an external magnet.

GRAPHICAL ABSTRACT

1. INTRODUCTION

As compared to other organic pollutants in wastewater, dyes are the least biodegradable organic pollutants and the textile industry is the major contributor to the contamination of the aquatic environment with dyes. Research findings have shown that dyes are carcinogenic compounds that have detrimental effects on the health of aquatic life and mammalian population (Núñez *et al.* 2019). Most of the dyes are not degraded during the conventional wastewater treatment processes, especially those that are classified as reactive, direct, basic, and acidic, since they have high solubility in water (Hassan & Carr 2018) and also they contain complex aromatic molecular structures (Zhang *et al.* 2016).

Diverse technologies are available to treat textile wastewater, and among them adsorption is effective to remove dyes from textile wastewater using activated carbon. Commercially available activated carbon is very effective to remove dyes; however, its high price limits its use, especially in developing countries for treatment of textile wastewater (Topare & Bokil 2020). Currently, researchers are interested in developing new adsorbent materials with low cost, various compositions, and selective functionalities (Danish *et al.* 2018), and hence, the need to develop low-cost adsorbent from agricultural by-products are increasing in demand (Pagalan *et al.* 2020).

Coffee is regarded as one of the most popular beverages throughout the world, and its consumption is constantly increasing. According to the International Coffee Organization (ICO), global coffee consumption was about 166.346 million 60 kg bags in 2020/21 and in 2019/20 164.202 million 60 kg bags. The trend shows an increase by about 1.3% (ICO 2021). It has been estimated that over 3.5 billion cups of coffee are served each day at the world level (Caetano *et al.* 2017), and more than 50 countries are involved in the commercial production of coffee (Rajesh Banu *et al.* 2020). During the processing of coffee, large amounts of solid residues are generated in the form of coffee pulp, coffee silver skin, spent coffee grounds (SCG), and coffee husk. SCG is an insoluble residue or waste product generated after milling and brewing during coffee beverage production (Rajesh Banu *et al.* 2020). On average, about 650 kg of SCG is generated from one tonne of green coffee beans, and approximately 2 kg of wet SCG is obtained during preparation of 1 kg of soluble coffee (Murthy & Naidu 2012). Therefore, globally, the amount of SCG generated from green coffee beans is approximately 6.5 million tonnes.

SCG causes problems during disposal at the landfill site as it has high oxygen demand during decomposition and contains toxic substances such as tannins, polyphenols, and caffeine, so disposal into the environment causes significant contamination (Rajesh Banu *et al.* 2020). It has been estimated that during the decomposition of one tonne of SCG, about 340 m^3 of methane gas is emitted to the environment (Ferreira and Ferreira 2019). Moreover, SCG are rich in organic components such as polysaccharides, oligosaccharides, lipids, lignin, proteins, alkaloids, amino acids, aliphatic acids, melanoidins, trigonelline, and volatile compounds. Thus direct disposal of SCG in landfills can create ecotoxicological concerns and environmental problems (Atabani *et al.* 2021).

Waste valorization is perceived as the process of transformation of wastes or agricultural by-products into value-added products by making use of processing technologies such as acid/alkaline hydrolysis, pyrolysis, fermentation, and anaerobic digestion (Lin *et al.* 2020). Therefore, one of the benefits of valorization is to implement efficient waste management as a fundamental solution for sustainable development. Pyrolysis can be described as a thermochemical process in which biomass is thermally decomposed to form its chemical constituents under inert or very limited oxygen supply. As compared to combustion, it is more efficient and results in less pollution (Tripathi *et al.* 2016).

Research findings have shown that chlorides of transition metals such as $FeCl_3$, $ZnCl_2$, etc. can modify the thermo-chemical behavior of certain hydrocarbon compounds through a coordination effect and result in the formation of crosslinking and carbonization of biomass (Sun *et al.* 2013). The use of $FeCl_3$ during carbonization of biomass significantly increases the degradation of both cellulose and hemicellulose, and its catalytic activity was higher than the chlorides of alkali metals and alkaline earth metals (Liu *et al.* 2009). Iron(III) salt enhanced the formation of aromatic structure during biomass carbonization process and hence provided adsorption sites for both polar and nonpolar organic contaminants (Han *et al.* 2021).

In this study, we developed an adsorbent prepared via one-step catalytic carbonization of spent coffee ground where iron chloride ($FeCl_3$) was used as a catalyst under limited air supply. The purpose of this study was management of SCG waste by valorization of SCG through pyrolysis, and the biochar obtained was used as adsorbent for the removal of textile dye (Vivizole Red 3 BS). The synthesized biochar composite adsorbent was characterized using different techniques to propose the removal mechanism of the dye, and the study would optimize the dye removal by making use of varied combination of the process parameters. To the best of our knowledge, the use of SCG biochar to remove Vivizole Red 3BS has not been tested before as such to offer both the management of the SCG waste and the textile wastewater treatment. Moreover, isotherm, kinetics, and thermodynamic studies were conducted for the adsorption of the dye by SCG biochar.

2. MATERIALS AND METHODS

2.1. Sorbate and adsorbent preparation

The molecular structure of Vivizole Red 3BS dye is shown in Figure 1. The stock solution of the dye was prepared (1,000 mg/L) by dissolving the dye in deionized water. The concentrations used in each run were obtained by dilution of the stock solution prepared.

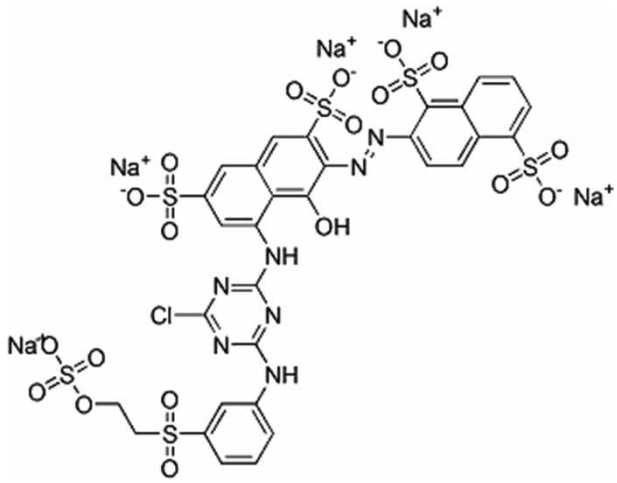

Figure 1 | Molecular structure of Vivizole Red 3BS dye.

SCG was obtained from ROBERA PLC, a coffee and roasted coffee processing company (Addis Ababa). With some modification, the procedure for one-step activation and synthesis of biochar was adopted (Wen *et al.* 2019), where iron (III) chloride serves as a catalyst for the carbonization of SCG and also result in the formation of magnetic biochar. The collected SCG was pre-treated with hot water, washed thoroughly with distilled water to

remove impurities such as dust and water-soluble substances from the surface of SCG, and dried at 105 °C for 24 hours. The dried fraction was pulverized and 10 g of SCG was added into 40 ml deionized water and 2 g of $FeCl_3$ was added and then soaked for about 30 min, followed by magnetic stirring at 80–85 °C for 120 min to vaporize water. The solid was dried at 70 °C in vacuum oven to get a constant mass carbon composite ready for the process of pyrolysis. The process of carbonization was carried out in a carbolite furnace (ELF 11/14B, UK). Samples were carbonized at the temperature of 750 °C under limited air at a heating rate of 10 °C min^{-1} and withholding time of 60 min. The sample was taken out of the furnace and cooled to room temperature. Without the addition of $FeCl_3$ salt, SCG was activated by following the above procedure and referred to as SCG0. The biochar samples were washed with deionized water several times and stored in drying oven at 30 °C and ready for further use.

2.2. Adsorbent characterization

To identify functionalities present within the SCG biochar, Fourier transform infrared (FTIR) (Spectrum 65, PerkinElmer) spectra were used. The total surface area of SCG biochar was determined by the Brunauer-Emmett-Teller (BET) method. Powder X-ray diffraction (Rigaku MiniFlex 600 Benchtop) was used to determine crystalline structure of the biochar sample. The pH at point of zero charge (pH_{PZC}) of the prepared adsorbents was measured using the drift method (Tran *et al.* 2016).

2.3. Design of experiment

Preliminary experiments were carried out to select the appropriate operating range for each of the factors used in the batch adsorption study. Through the central composite design (CCD) of the response surface methodology (RSM) using Design Expert 11.0 software, 30 runs with varied combination of the factor chosen (contact time:10–120 min, adsorbent dose: 4–12 g/L, initial dye concentration: 10–50 mg/L, and pH: 3–11) were generated and analyzed in the experiment. The experimental levels of independent variables and their coded values are shown in Table 1. To predict the response, i.e., percent dye removal; the quadratic surface polynomial model was used as given in Equation (1).

Table 1 | Coded and actual variables and their level in CCD

		levels		
Code	**Variable**	**(−1)**	**(0)**	**(+1)**
A	Initial dye concentration (mg/L)	10	30	50
B	pH	3	7	11
C	Dose (g/L)	4	8	12
D	Contact time (min.)	10	65	120

$$Y = \beta_0 + \sum_{i=1}^{n} \beta_i X_i + \sum_{i=1}^{n} \beta_{ii} X_i^2 + \sum_{i=1}^{n-1} \sum_{j=i+1}^{n} \beta_{ij} X_i X_j \quad (1)$$

where Y represent the response; (X_i and X_j) denote the independent variables; β_0 is a constant number, β_i. β_{ii} and β_{ij} represent linear, quadratic coefficient, and interactive terms, respectively (Bayuo *et al.* 2020). Therefore, the response surface method based on the CCD was used to evaluate the outcome of independent variables on the response function.

2.4. Modeling and optimization

The effects of the most influencing factors were analyzed by making use of analysis of variance (ANOVA) to determine the possible combinations of the factors that would give the best model for the adsorption of the dye by SCG biochar. The best result of numerical optimization was validated through experimental runs in the laboratory. In the analysis, the significant factors ($p \leq 0$) affecting the adsorption of the dye by SCG biochar were determined and the most fitted model was given as surface quadratic equation. The effects of the significant

factors were analyzed and presented through contour plots and 3D models generated by Design Expert 11.0 software.

2.5. Adsorption experiments

Batch adsorption experiments were carried out by shaking a known amount of adsorbent in 50 mL of dye solution with different concentration in a 100 mL conical flask. At a predetermined adsorption time, each dye sample was withdrawn from the adsorption solution and centrifuged for 20 min at 4,000 rpm to separate the used adsorbent from the dye solution, and the amount of each dye in the supernatant was determined by measuring the absorbance at the λ_{max}. using UV/Vis spectrophotometer (1,600 Series Single Beam) (λ_{max} for Vivizole Red 3BS is 540 nm).

Amount of each dye adsorbed at time t and at equilibrium will be given by Equations (2) and (3), respectively:

$$q_t = \frac{(C_0 - C_t) * V}{m} \tag{2}$$

$$q_e = \frac{(C_0 - C_e) * V}{m} \tag{3}$$

where C_0, C_t and C_e. are initial, final, and equilibrium concentrations of the dye in mg/L, respectively, V is volume of a solution in liter, and m is the mass of adsorbent in g/L.

The percentage of dye removal can be computed by Equation (4):

$$\textit{Removal rate } (\%) = \frac{C_0 - C_f}{C_0} \tag{4}$$

where C_f is final concentration of the solutn.

2.6. Adsorption isotherm

The adsorption isotherm study was conducted based on the optimum values obtained in batch adsorption experiments. Batch adsorption kinetics experiments were carried out in 100 mL conical flask by taking 50 mL of dye solution and agitating with water bath shaker at a temperature of 30 °C. Hence optimum adsorbent dose and contact time were used by varying the initial dye concentrations (10, 15, 20, 25, and 30 mL). The data were fitted to the Langmuir, Freundlich, Redlich–Peterson and Toth models given by nonlinear equation forms (5), (6), (7) and (8), respectively:

$$q_e = \frac{K_L q_L C_e}{1 + K_L C_e} \tag{5}$$

where q_L: maximum monolayer coverage capacity (mg/g); K_L: Langmuir isotherm constant; C_e: equilibrium concentration (mg/L); and q_e: the amount of dye adsorbed when saturation is achieved (mg/g).

$$q_e = k_F (C_e)^{\frac{1}{n}} \tag{6}$$

where k_F: the Freundlich isotherm constants (mg/g) representing adsorption capacity and n: Freundlich intensity parameter.

$$q_e = \frac{K_R C_e}{1 + a_R (C_e)^g} \tag{7}$$

where a_R: Redlich-Peterson isotherm constant (L/mg); g: Redlich-Peterson isotherm exponent located between 0 and 1; K_R: Redlich-Peterson isotherm constant (L/g)

$$q_e = \frac{K_T C_e}{(a_T + C_e)^{\frac{1}{t}}} \tag{8}$$

where a_T: Toth isotherm constant (L/mg); K_T: Toth isotherm constant (m/g); t: Toth isotherm constant.

2.7. Thermodynamics

Adsorption thermodynamics of the SCG biochar was investigated by making use of the change in Gibbs standard free energy (ΔG^0), standard enthalpy (ΔH^0), and standard entropy (ΔS^0) given by Equations (9) and (10).

$$\Delta G^0 = -RT \ln K_D \tag{9}$$

$$\ln K_D = -\frac{\Delta H^0}{RT} + \frac{\Delta S^0}{R} \tag{10}$$

where R is the gas constant (8.314 J·mol^{-1} K^{-1}), T is the adsorption temperature in kelvin, K_D is the thermodynamic equilibrium constant that was obtained as shown in Equation (11)

$$K_D = \frac{q_e}{C_e} \tag{11}$$

ΔS^0(J mol^{-1} K^{-1}) and ΔH^0 (kJ mol^{-1}) was determined from the intercept and slope of a linear plot ln K_D versus 1/T, and the values of ΔG^0 at the following temperatures (298, 303, and 308 K) were calculated.

2.8. Adsorption kinetics

Kinetic studies help to predict the adsorption mechanism and to determine the potential steps which control the adsorption rate, such as chemical reaction and mass transport processes (Anastopoulos *et al.* 2018). Several kinetic models are available; however, pseudo-first- and pseudo-second-order kinetic equations are the most commonly used in adsorption studies (Awad *et al.* 2020). Pseudo-first- and second-order models were applied for this particular study. Moreover, to find out whether the process of adsorption is controlled by diffusion or not, an intraparticle diffusion kinetic model (Benjelloun *et al.* 2021) was also used.

Batch adsorption kinetics experiments were carried out in 100 mL conical flask by taking 50 mL of dye solution and agitating with water bath shaker at temperature of 30 °C. Optimum operating conditions with contact times of 30, 55, 80, 105, 130 and 155 min were used. The data obtained was fitted to pseudo-first-, pseudo-second-order and intraparticle diffusion kinetic models as shown in Equations (12)–(14) below, respectively.

$$ln(q_e - q_t) = ln(q_e) - k_1 t \tag{12}$$

$$\frac{t}{q_t} = \frac{1}{k_2\, q_e^2} + \frac{t}{q_e} \tag{13}$$

$$Q_t = K_{ID}\sqrt{t} + I \tag{14}$$

where t is contact time in hour (h), k_1 is the first order rate constant (h^{-1}), and k_2 is the rate constant of second-order (h/L), Q_t is the amount of adsorbate in the aorbent at time t (mg/g), K_{ID} is intraparticle diffusion rate constant, t is time of contact (min) and I intercept of intraparticle diffusion kinetic model.

3. RESULTS AND DISCUSSION

3.1. Characterization of biochar composite

The FTIR spectra analyses can provide some valuable information about identification of chemical species of the SCG biochar. Functional groups on the surface of biochar can influence the adsorption performance of the biochar formed with and without addition of $FeCl_3$. Even without the addition of iron(III) salt, increasing pyrolysis temperature would decrease hydrogen content (H%); however, the carbon content (C%) of biochar increases with increasing pyrolysis temperature (Xiao *et al.* 2018). Therefore, the addition of iron(III) salt significantly decreases the H/C ratio and it has been suggested that iron(III) facilitates the formation of aromatic structure. The presence of Fe-O bond vibration of Fe_3O_4/Fe_2O_3 can be corroborated by FTIR analysis; however, the characteristic peaks of Fe-O bond depend of the sources of biochar and its preparation methods (Shin *et al.* 2021; Zeng & Kan 2021). Generally, as observed in Figure 2, the presence of metal oxides such as Fe-O and Fe-O-Fe on the surface of biochar is indicated in the ranges of 730–500 cm^{-1} (Liang *et al.* 2021). Whereas in the case of pristine SCG biochar (Figure 2) no visible peak is observed in the aforementioned range.

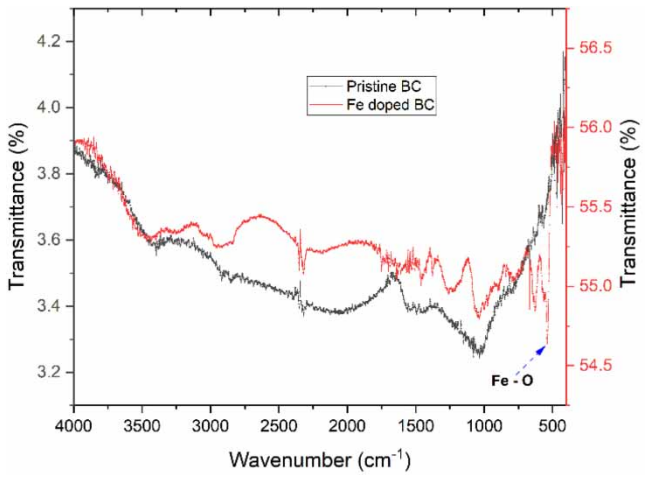

Figure 2 | FTIR spectrum of pristine and Fe doped biochar.

The broad band between 3,500 cm^{-1} and 3,300 cm^{-1} represents O-H stretching vibration of hydroxyl groups of alcohols (Peng *et al.* 2018). However, as depicted in Figure 2, the O-H stretching vibration band was very low and this suggests that oxygen was removed significantly during carbonization process and phenolic-aromatic structures were converted to form carbon materials. Moreover, the process of activation and thermal treatment promoted the conversion to graphitic structure (Tomin *et al.* 2021). The C = C band of aromatic rings appeared in the range between 1,650 and 1,470 cm^{-1} (Shin *et al.* 2021). There is also a peak at 879 cm^{-1}, which confirmed the out-of-plane bending of the = C-H in the aromatic ring (Yao *et al.* 2020). The peak at 1,150–1,050 cm^{-1} shows the C – O stretching of ethers (Shin *et al.* 2021) and the characteristic vibration band around 1,000 cm^{-1} is assigned to C – O – C (Liang *et al.* 2021).

The XRD technique is used to indicate the structure of crystal and phase composition of the materials. The existence of Fe-O bond is further indicated by XRD (S 1). Two strong peaks at around 30.16° and 35.52° were assigned to Fe_3O_4 and which are related to the (220) and (311) planes, respectively (Dong *et al.* 2017).

The point of zero charge pH (pH_{pzc}) can be described as the pH value at which the surface charge of the adsorbent is zero and it shows the comprehensive effects of the different functional groups on the biochar surface.[73] The pH_{pzc} of biochar prepared without addition of iron(III) salt was 8.1, whereas pH_{pzc} of biochar obtained from the addition of iron(III) salt was 3. The yield of SCG-Fe biochar was 20%, whereas the biochar obtained from pristine SCG was 22%. Yield reduction for SCG-Fe biochar is due to addition of iron(III) salt (Han *et al.* 2021) since it facilitates the process of graphitization (Tomin *et al.* 2021). The BET area of pristine SCG biochar was 128 m^2/g, whereas the BET value of SCG-Fe biochar was 89 m^2/g. Reduction in BET value could be attributed to the closing or blockage of pores by metal oxide on the surface of biochar (Nguyen *et al.* 2021).

3.2. Predictive model for the removal of VR3BS dye by biochar composite

The parametric interactions and impacts of their interactions on the response were investigated with RSM-CCD (Table 2) and described in terms of the coded parameters by the second-order polynomial regression model given by Equation (15).

$$\textit{Percent removal}\ (Y) = 53.04 - 19.56A + 0.622B + 20.26\,C + 1.41D - 0.26AB - 2.70\,AC - 1.1\,AD + 0.24BC + 0.21BD - 0.58CD + 16.04\,A^2 - 2.41B^2 - 7.4\,C^2 - 1.71D^2 \quad (15)$$

Table 2 | Model summary statistics for adsorption capacity of biochar for VR3BS dye

Source	Sequential *p*-value	Lack of fit *p*-value	R^2	Adjusted R^2	Predicted R^2	Comment
Linear	<0.0001	0.0691	0.9283	0.9169	0.9066	
2FI	0.8188	0.0470	0.9377	0.9049	0.8952	
Quadratic	<0.0001	0.4867	0.9861	0.9731	0.9492	Suggested
Cubic	0.5839	0.3023	0.9930	0.9710	0.6693	Aliased

The second-order polynomial regression equation generated by CCD was validated by considering results in actual runs, as shown in S2. The ANOVA was used to determine the reliability of the model developed (Table 3). The model F-value of 76.06 implies that the model is significant and there is only a 0.01% chance that an F-value this large could occur due to noise. The result of ANOVA showed that the following parameters and an interaction effect were significant model terms: A, C, AC, A^2, and C^2, and all parameters and their interaction effects were not significant. According to the F-value (Table 3), two parameters had a significant effect on the removal of the dye. The F-value of dose (C) and initial dye concentration (A) were higher at about 517 and 482, respectively, and this implied the two had most significant influence on the percent of dye removal (Bayuo *et al.* 2020).

Table 3 | ANOVA reliability test for the quadratic surface model used to estimate removal of VR 3BS dye using SCG biochar

Source	Sum of squares	Df	Mean square	F-value	*p*-value
Model	15, 206.26	14	1086.16	76.06	$< 0.0001^a$
A-Initial Dye Conc.	6,887.47	1	6887.47	482.33	$< 0.0001^a$
B-pH	6.97	1	6.97	0.4880	0.4955^b
C-Dose	7,385.18	1	7385.18	517.18	$< 0.0001^a$
D-Contact time	35.84	1	35.84	2.51	0.1340^b
AB	1.10	1	1.10	0.0772	0.7849^b
AC	116.64	1	116.64	8.17	0.0120^a
AD	19.36	1	19.36	1.36	0.2625^b
BC	0.9025	1	0.9025	0.0632	0.8049^b
BD	0.7225	1	0.7225	0.0506	0.8251^b
CD	5.29	1	5.29	0.3705	0.5519^b
A^2	666.26	1	666.26	46.66	$< 0.0001^a$
B^2	15.10	1	15.10	1.06	0.3201^b
C^2	142.42	1	142.42	9.97	0.0065^a
D^2	7.61	1	7.61	0.5331	0.4766^b
Residual	214.19	15	14.28		
Lack of Fit	147.36	10	14.74	1.10	0.4867^b
Pure Error	66.83	5	13.37		
Cor Total	15,420.45	29			
$R^2 = 0.986$					

[a] = significant; [b] = not significant; Df, Degree of freedom.

The second-order polynomial model Equation (15) was reduced to Equation (16) after removing the nonsignificant model terms.

$$\textit{Percent removal}\ (Y) = 53.04 - 19.56A + 20.26\ C - 2.70\ AC + 16.04\ A^2 - 7.4\ C^2 \quad (16)$$

According to the second-order polynomial model, when the value of the initial dye concentration (A) increased, the percent dye removal decreases. The percent removal of the dye decreases with increase of initial dye concentration if the active sites on the surface of the biochar are saturated (Yu *et al.* 2021). The interaction between initial dye concentration and dose (C) and the square of dose have negative coefficients in the range tested for the removal of VR 3BS dye and have negative effect on the removal of dyes. However, the dose alone and the squared value of initial dye concentration favored the percent removal of the dye. The lack of fit *p*-value of the model is insignificant, and the value of regression coefficient (R^2) was high (0.986). Moreover, the values of adj R^2 and pred R^2 were well within 20% of each other (Table 2) and provide 94.92% of variability to predict new observations as compared to approximately 97.31% variability in the original data (Rai *et al.* 2016).

Based on the result of the ANOVA, the F-value for the model was significant, and there was a good correlation between the response and the independent variables of the model and also the sum of squares (SS) values of the variables were high (Table 3), implying the importance of the variables (Jaafari *et al.* 2020). Adequate precision is used to measure the signal to noise ratio and compares the ranges of predicted values of the design point in comparison to the average predicted error. A ratio greater than 4 is desirable, and for this particular work the ratio is 31.392 indicating an adequate signal, and this model can be used to navigate the design space. The coefficient of variation (CV = 6.78) and standard deviation (SD = 3.78) reflect the degree of precision of the measurements. The low values of SD and CV show that the measurements conducted are adequate (Mourabet *et al.* 2017), thus the model was efficient in predicting the percent removal of VR 3BS dye, so the model can justify 98.6% of data variation (Pagalan *et al.* 2020).

The ANOVA result showed that among the available interactive effects; only the initial dye concentration (A) and adsorbent dose (C) have significant interactive effects on the percent removal of VR 3BS dye with SCG biochar. Therefore, the interactive effect of AC was the one only described (Figure 3).

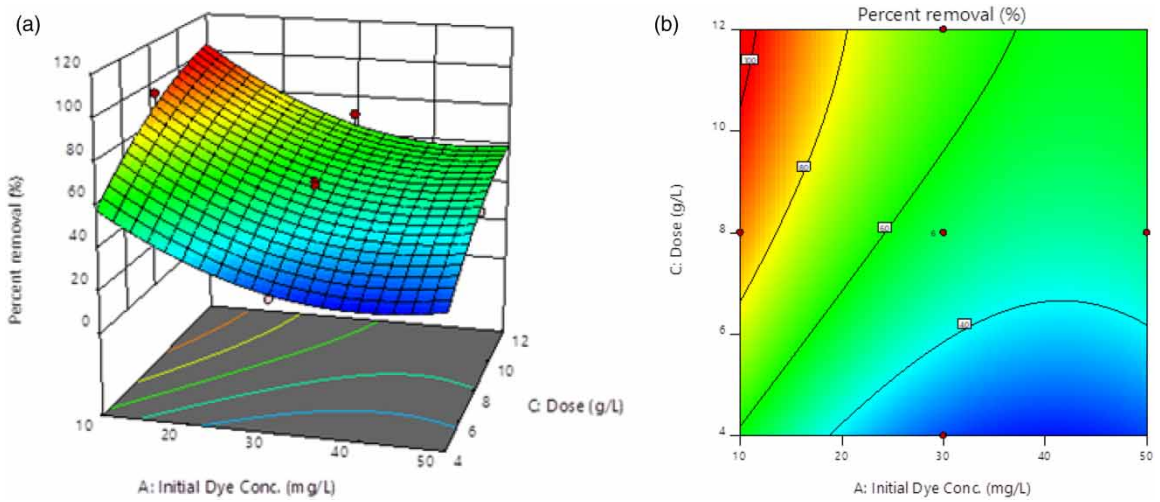

Figure 3 | (a) 3D response surface plot and (b) contour plot of VR3BS dye removal showing interaction of dose and initial dye concentration.

According to the 3D response surface plot indicated in Figure 3(a) and 2D contour shown in Figure 3(b) for the interaction of dose of adsorbent and initial dye concentration, low dose at higher dye concentration resulted in the decreased percent removal of VR 3BS dye. At lower initial dye concentration, the percent removal of the dye increased when dose of adsorbent was higher. This was mainly because as the ratio of the number of dye molecules to the available active sites on the adsorbent is low, there is a greater possibility of interaction between the molecules of the dye and available active sites on the biochar (Gebreslassie 2020). As the ratio of a number of dye molecules to the number of surface-active sites on the biochar increases, the active sites on the biochar saturated, and the percentage removal of the dye decreases.

Graphs can be used to validate CCD model by evaluating correlation between actual and predicted values and the nature of residual distribution. As indicated in S3 (a), in the relationship between actual and predicted values, there were minimum divergence of points from the straight diagonal line (Jawad *et al.* 2020). As shown in S3 (b), the normal probability of residuals values pattern also follows along the straight line and thus indicating ideal distribution and independence of residuals (Sharifpour *et al.* 2020). In S3(c), all the experimental data points were within the residual limits (± 4) (Ghoreishian *et al.* 2019), and indicating that the proposed model was adequate and satisfied the constant variance assumption. Therefore, the RSM-CCD model equation can be used to sufficiently describe the interaction of the independent variables under study.

3.3. Optimum conditions of VR3BS dye removal using the biochar composite

This study employed input variables with specific ranged values whereas the response, i.e., percent removal of VR 3BS dye, was assigned to achieve maximum value. The suggested optimum values of CCD were 10 ppm initial

concentration of VR3BS dye, 1 g per 100 ml adsorbent dose, and contact time of 101 min with optimum predicted dye removal of 99%. Validation of experimental runs was carried out using the optimum conditions in triplicate and the average value of percent removal of VR3BS was 97.2% (Table 4). However, the removal efficiency of biochar obtained from pristine SCG is only 60%.

Table 4 | Optimization and validation results of VR3BS dye adsorption

	Factor				Response
Optimization/Experiment	Initial dye conc. (ppm)	pH	Adsorbent dose (g/L)	Contact time (Min.)	VR 3BS dye removal (%)
CCD-RSM[a]	10	8	10	101	99
Validation	10	8	10	101	97.2
SCG Biochar[b]	10	8	10	101	60

[a]Optimization criteria: initial dye concentration (10–50 ppm), pH (3–11), dose of adsorbent (4–12 g/L) and contact time (10–120 min) were in range and percent dye removal was maximized.
[b]Control run without activating agent.

3.4. Adsorption isotherm studies

Equilibrium isotherm studies can be used to get information about the distribution of adsorbate molecules at the solid/liquid interface. In this study, the equilibrium data of VR3BS dye adsorption with the optimized SCG biochar were fitted to Langmuir, Freundlich, Temkin and Redlich–Peterson models, and the resulting isotherm parameters values calculated from the fitting are shown in Table 5. The Langmuir isotherm was the most fitted isotherm model with the adjusted R^2 value of 0.986 (Figure 4(a)) and followed by Toth isotherm ≈ Redlich – Peterson isotherm and then Freundlich isotherm. The adsorption of VR3BS dye follows the Langmuir isotherm model. Adsorption of dyes by both physically and chemically activated SCG also followed the Langmuir isotherm model (Lim *et al.* 2016; Wirawan *et al.* 2020). Since the Langmuir isotherm model assumes a monolayer type of adsorption on homogeneous surfaces, there are limited number of adsorption sites (Rangabhashiyam *et al.* 2014). Therefore, the adsorption capacity of SCG biochar activated with iron(III) salt was 2.07 mg/g.

Table 5 | Equilibrium isotherm model parameters calculated from VR3BS dye using optimized SCG biochar

Adsorption Isotherm	Parameter	Value	R^2
Langmuir	q_m (mg/g)	2.07	0.986
	k_L (L/mg)	0.832	
Freundlich	k_f $(mg/g)(L/g)^n$	1.03	0.925
	n	0.26	
Redlich–Peterson	K_R (L/g)	1.713	0.978
	a_R $(L/mg)^g$	0.895	
	g	0.987	
Toth	K_T (mg/g)	1.97	0.979
	a_T	1.12	
	t	0.986	

3.5. Adsorption thermodynamics

The thermodynamic parameters of the adsorption process of VR3BS dye by SCG biochar activated with iron(III) salt were investigated at three different temperature values and the calculated values of ΔG^0, ΔS^0 and ΔH^0 are listed in Table 6.

The obtained values for Gibbs free energy change (ΔG^0) are negative, which indicate that the adsorption process is spontaneous and thermodynamically favored (Theydan & Ahmed 2012). The strength of the adsorption

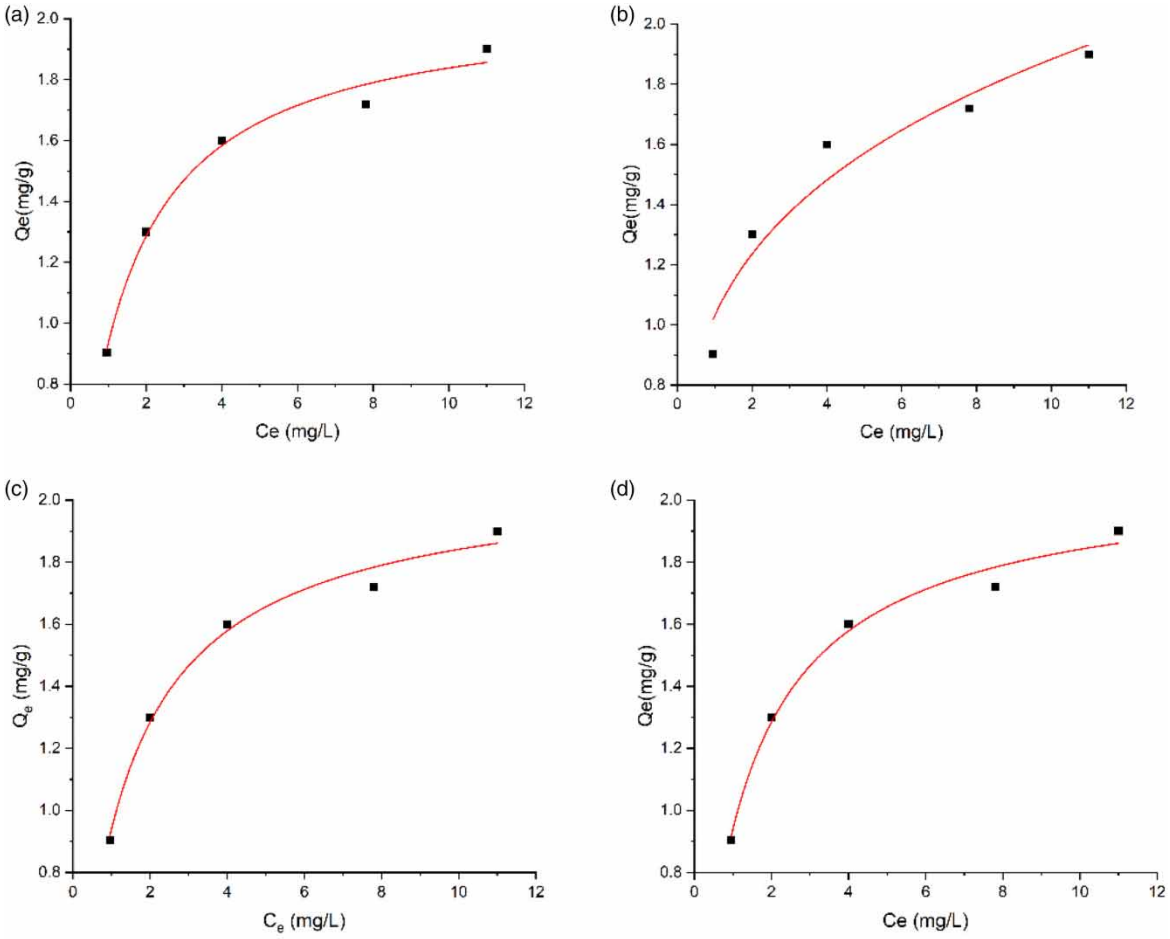

Figure 4 | Isotherm plots of (a) Langmuir, (b) Freundlich, (c) Redlich–Peterson, and (d) Toth models.

Table 6 | The thermodynamic parameters for the adsorption of VR3BS by SCG biochar composite

Temperature (K)	K_D	ΔG^0 (KJ mol^{-1})	ΔS^0 (KJ mol^{-1})	ΔH^0(KJ mol^{-1})
298	1.04	−0.105	567.73	169.21
303	2.74	−2.542		
308	9.6	−5.792		

process increases with temperature (Ma *et al.* 2021a). The calculated enthalpy and entropy values were both positive and confirmed that the process of adsorption of VR3BS dye by the SCG biochar composite is endothermic (Liu *et al.* 2019). Based on the ranges of free energy (ΔG^0) values, adsorption process can be categorized as physisorption and chemisorption, and the range for physisorption is between −20 and 0 kJ/mole, whereas for chemisorption it is between - 80 and - 400 kJ/mol (Abdelwahab & Amin 2013). Therefore, the value of ΔG^0 for the adsorption of VR3BS dye by SCG biochar was in the range of physisorption. However, the enthalpy of adsorption for physisorption is the range of 2.1–20.9 KJ/mol, whereas for chemisorption it falls within the range of 80–200 KJ/mol (Nnadozie & Ajibade 2021). The enthalpy of adsorption of VR3BS dye on SCG biochar composite was 169.21 KJ/mol and it has been suggested that the adsorption process was neither purely physisorption nor chemisorption. The values of $\Delta S^0 > 0$ indicates that there is randomness on the solid-solution interface and this implies that the molecular structure of adsorbate and the adsorbent surface had changed to some extent during the process of adsorption (Ma *et al.* 2021b). Therefore, thermodynamic study revealed that the adsorption process was spontaneous, favourable, endothermic and physicochemisorption in nature.

3.6. Adsorption kinetic studies

Kinetic study provides a better insight to elucidate the process of adsorption phenomena. To determine the potential steps which control the adsorption rate and type, the fitting of the process to pseudo-first, pseudo-second and intraparticle diffusion kinetic models were evaluated (Benjelloun *et al.* 2021; Grisales-Cifuentes *et al.* 2021). Optimum operating conditions with contact times of 30, 55, 80, 105, and 155 min were used. The parameters of kinetic data analysis for the adsorption of VR3BS dye on SCG composite biochar are shown in Table 7 and the plots are given in Figure 5(a)–5(c).

Table 7 | Kinetic model parameters for the adsorption of VR3BS dye by SCG biochar composite

Kinetic model	Parameter/Value	
Pseudo-first-order	q_e (mg/g)	1.19
	K_1	2.77E-6
	R^2	0.86
Pseudo-second-order	q_e (mg/g)	0.96
	K_2	0.07
	R^2	0.999
Intra-particle diffusion	K_{diff}	0.0092
	R^2	0.93

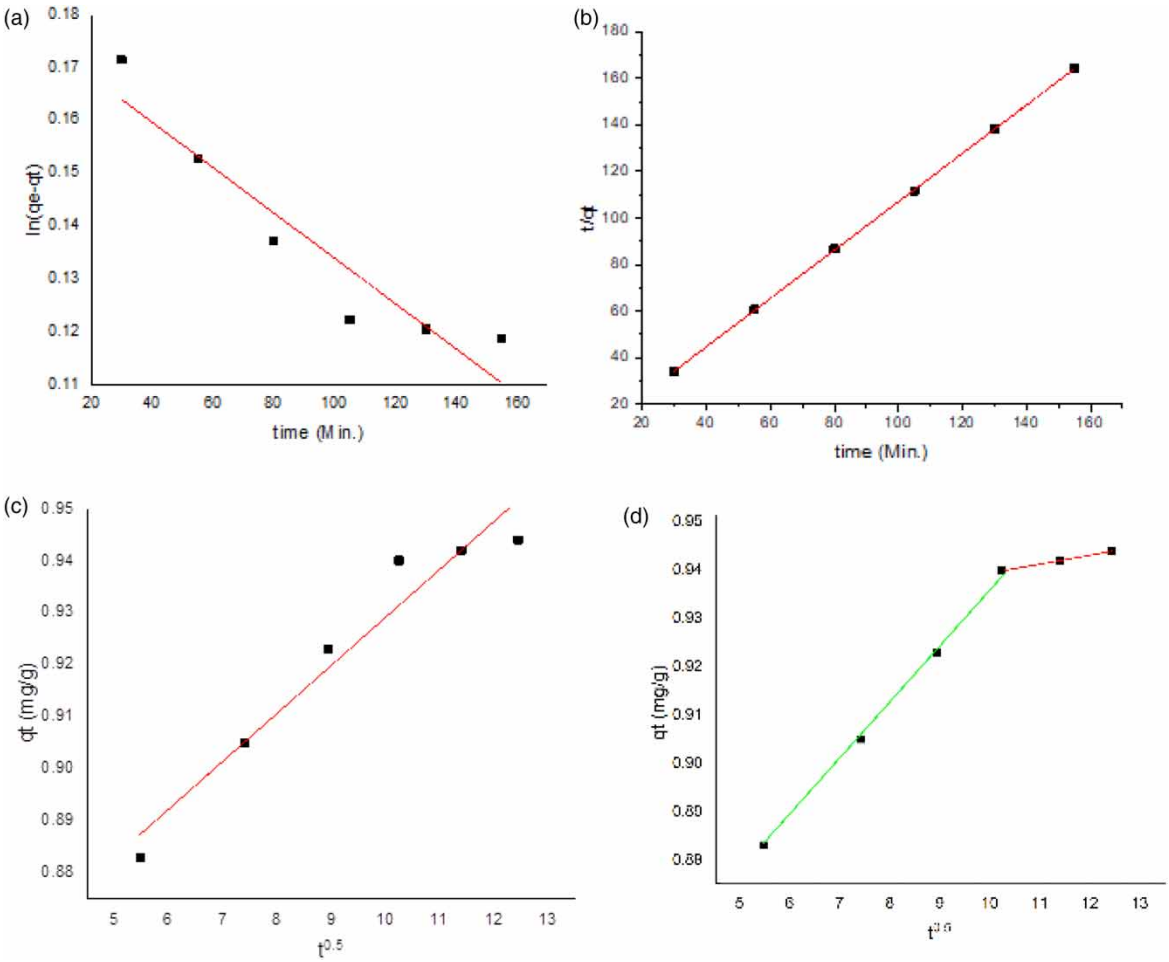

Figure 5 | The plot of kinetic models (a) pseudo-first-order, (b) pseudo-second-order and (c) and (d) intraparticle diffusion for the adsorption of VR3BS dye on SCG biochar composite.

Adsorption kinetics was better described by the pseudo-second-order model, and it was suggested that the rate of adsorbate–adsorbent interaction is dependent on both the amount of dye adsorbed at the biochar surface and the adsorbed amount at equilibrium (Grisales-Cifuentes *et al.* 2021).

Intraparticle diffusion model was used to describe the nature of adsorption mechanisms influencing the adsorption of VR3BS dye onto the biochar. In Figure 5(c), the regression line is not linear from the origin and thus intraparticle diffusion is not the only rate limiting step (Yao *et al.* 2020). As indicated in Figure 5(d), two distinct linear segments with different slopes were observed. The first phase of adsorption, i.e., from $t = 0$ to 105 min, is faster and corresponds to liquid film diffusion and the second phase, from $t \geq 105$ min, is controlled by intra-particle diffusion and is delayed phase. It was pointed out that the diffusion resistance across the liquid boundary layer is smaller than the resistance during the pore diffusion phase (Sumalinog *et al.* 2018).

3.7. Adsorption mechanisms of VR3BS dye

Determination of the adsorption mechanism is very important in controlling the adsorption process. However, this is not an easy task since the adsorption mechanism is a complicated process governed by many factors such as the porosity, surface area, surface charge, pH, functional groups, carbon and aromatic content, and mineral composition of the biochar (Liu *et al.* 2018; Doan *et al.* 2021). Varieties of mechanisms were proposed for the adsorption of organic pollutants onto biochar. Pore-filling, hydrophobic, and electrostatic interactions and hydrogen bonding are considered the major mechanisms that are responsible for the adsorption between organic contaminants and biochar. Iron(III) employed as a catalyst during the carbonization of SCG has good graphitization efficiency and the onset of the graphitization by Fe takes place starting from 715 °C (Gomez-martin *et al.* 2021). Therefore, the aromatic structure in graphite provides adsorption sites for both polar and nonpolar organic contaminants. Among others, the possible adsorption mechanism is π – π electron donor–acceptor (EDA) interactions between the dye molecules and the aromatic group in the graphite structure of biochar (Wen *et al.* 2019; Liu *et al.* 2021). The results of FTIR analysis show that the surface of the biochar contains functional groups such as – OH, – CO, and – CH, which are responsible for the adsorption of VR3BS dye through π – π interaction and hydrogen bonding, etc. Since the addition of iron(III) enhanced the formation of the aromatic structure of biochar (Han *et al.* 2021), the dye with an aromatic structure could be adsorbed onto the biochar through π – π EDA interactions, and hydrogen bonding is formed between the N atoms on the dye molecule and the oxygen-containing functional groups of the biochar (Yao *et al.* 2020). The intraparticle diffusion model confirms that diffusion into adsorbent pores is not the only mechanism governing the adsorption process. Moreover, the results from the thermodynamic study suggest that the adsorption of VR3BS dye by SCG–Fe biochar involves both physisorption and chemisorption mechanisms.

4. CONCLUSION

Coffee consumption is increasing throughout the world, and a significant amount of solid residue generated in the form of SCG is disposed of in landfill sites and thus responsible for the environmental problems. Valorization of SCG through pyrolysis could be the solution to this challenge and the biochar obtained was used as an adsorbent for the removal of the textile dye–Vivizole Red 3 BS. Iron(III) salt was used as a catalyst during carbonization of SCG biomass and has a good graphitization efficiency and thus enhanced the formation of aromatic structures which provide adsorption sites for the dye. The yield of biochar was 20% when the SCG was pyrolyzed at 750 °C. A predictive model for the removal of the dye was investigated with RSM–CCD and the result of ANOVA showed that the two parameters, namely the dose of adsorbent and initial dye concentration had a significant effect on the removal of the dye. The suggested optimum values of the CCD were 10 ppm initial dye concentration, 1 g per 100 ml adsorbent dose, and contact time of 101 min with optimum predicted dye removal of 99%. However, the removal efficiency obtained from pristine biochar is only 60%. The Langmuir model was the most fitted isotherm model with an adsorption capacity of 2.07 mg/g. Adsorption kinetic equilibrium data was better described by pseudo-second-order model, and from the thermodynamic study, it has been suggested that the adsorption process was spontaneous, favourable, endothermic, and the nature of the removal involves both physical and chemical adsorption processes. The possible adsorption mechanisms governing the adsorption process of the dye with biochar are π – π electron donor-acceptor interaction and hydrogen bonding. Therefore, the biochar obtained from one-step catalytic pyrolysis of SCG waste can offer both the management of the SCG waste and for the treatment of textile wastewater.

ACKNOWLEDGEMENTS

The authors thank the Africa Centre of Excellence for Water Management. the Department of Chemistry, Addis Ababa University. The authors would like to extend thanks to Robera Plc, coffee and roasted coffee processing company, Addis Ababa, for the provision of SCG.

AUTHOR CONTRIBUTIONS

Admasu Adamu: conceptualization, methodology, visualization, investigation, writing original draft, review, and editing. Yonas Chebude: supervision, manuscript reviewing, and editing. Feleke Zewge: supervision.

CONFLICTS OF INTEREST

The authors declare that there are no conflicts of interest.

DATA AVAILABILITY STATEMENT

All relevant data are included in the paper or its Supplementary Information.

REFERENCES

Abdelwahab, O. & Amin, N. K. 2013 Adsorption of phenol from aqueous solutions by Luffa cylindrica fibers: kinetics, isotherm and thermodynamic studies. *Egypt. J. Aquat. Res.* **39**, 215–223.

Anastopoulos, I., Hosseini-Bandegharaei, A., Fu, J., Mitropoulos, A. C. & Kyzas, G. Z. 2018 Use of nanoparticles for dye adsorption: review. *J. Dispers. Sci. Technol.* **39**, 836–847.

Atabani, A. E., Ali, I., Naqvi, S. R., Badruddin, I. A., Aslam, M., Mahmoud, E., Almomani, F., Juchelková, D., Atelge, M. R. & Khan, T. M. Y. 2021 A state-of-the-art review on spent coffee ground (SCG) pyrolysis for future biorefinery. *Chemosphere* **286**, 131730.

Awad, A. M., Jalab, R., Benamor, A., Nasser, M. S., Ba-abbad, M. M., El-naas, M. & Wahab, A. 2020 Adsorption of organic pollutants by nanomaterial-based adsorbents: an overview. *J. Mol. Liq.* **301**, 112335.

Bayuo, J., Abukari, M. A. & Pelig-Ba, K. B. 2020 Optimization using central composite design (CCD) of response surface methodology (RSM) for biosorption of hexavalent chromium from aqueous media. *Appl. Water Sci.* **10**, 1–12.

Benjelloun, M., Miyah, Y., Akdemir Evrendilek, G., Zerrouq, F. & Lairini, S. 2021 Recent advances in adsorption kinetic models: their application to dye types. *Arab. J. Chem.* **14**, 103031.

Caetano, N. S., Caldeira, D., Martins, A. A. & Mata, T. M. 2017 Valorisation of spent coffee grounds: production of biodiesel via enzymatic catalysis with ethanol and a co-solvent. *Waste Biomass Valorization* **8**, 1981–1994.

Danish, M., Ahmad, T., Majeed, S., Ahmad, M., Ziyang, L., Pin, Z. & Iqubal, S. M. S. 2018 Use of banana trunk waste as activated carbon in scavenging methylene blue dye: kinetic, thermodynamic, and isotherm studies. *Bioresour. Technol. Reports* **3**, 127–137.

Doan, V. D., Tran, T. K. N., Nguyen, A. T., Tran, V. A., Nguyen, T. D. & Le, V. T. 2021 Comparative study on adsorption of cationic and anionic dyes by nanomagnetite supported on biochar derived from Eichhornia crassipes and Phragmites australis stems. *Environ. Nanotechnology, Monit. Manage.* **16**, 100569.

Dong, C., Chen, C. & Hung, C. 2017 Synthesis of magnetic biochar from bamboo biomass to activate persulfate for the removal of polycyclic aromatic hydrocarbons in marine sediments. *Bioresour. Technol.* **245**, 188–195.

Ferreira, J. & Ferreira, C. 2019 Seeking sustainability in the coffee shop industry: innovation in the circular econmy. In *The Centre for Business in Society White Paper Series*.

Gebreslassie, Y. T. 2020 Equilibrium, kinetics, and thermodynamic studies of malachite green adsorption onto Fig (Ficus cartia) leaves. *J. Anal. Methods Chem.* **2020**, 7384675.

Ghoreishian, S. M., Raju, G. S. R., Pavitra, E., Kwak, C. H., Han, Y.-K. & Huh, Y. S. 2019 Ultrasound-assisted heterogeneous degradation of tetracycline over flower-like rGO/CdWO4 hierarchical structures as robust solar-light-responsive photocatalysts: optimization, kinetics, and mechanism. *Appl. Surf. Sci.* **489**, 110–122.

Gomez-martin, A., Schnepp, Z. & Ramirez-rico, J. 2021 Structural evolution in iron-catalyzed graphitization of hard carbons. *Chem. Mater.* **33**, 3087–3097.

Grisales-Cifuentes, C. M., Serna Galvis, E. A., Porras, J., Flórez, E., Torres-Palma, R. A. & Acelas, N. 2021 Kinetics, isotherms, effect of structure, and computational analysis during the removal of three representative pharmaceuticals from water by adsorption using a biochar obtained from oil palm fiber. *Bioresour. Technol.* **326**, 124753.

Han, L., Sun, H., Sun, K., Yang, Y., Fang, L. & Xing, B. 2021 Effect of Fe and Al ions on the production of biochar from agricultural biomass: properties, stability and adsorption efficiency of biochar. *Renewable Sustainable Energy Rev.* **145**, 111133.

Hassan, M. M. & Carr, C. M. 2018 A critical review on recent advancements of the removal of reactive dyes from dyehouse effluent by ion-exchange adsorbents. *Chemosphere* **209**, 201–219.

ICO 2021 Word Coffee Consumption. In *Int. Coffee Organ. 2021*.

Jaafari, J., Barzanouni, H., Mazloomi, S., Amir, N., Farahani, A., Shara, K., Soleimani, P. & Ali, G. 2020 Effective adsorptive removal of reactive dyes by magnetic chitosan nanoparticles: kinetic, isothermal studies and response surface methodology. *Int. J. Biol. Macromol.* **164**, 344–355.

Jawad, A. H., Mohammed, I. A. & Abdulhameed, A. S. 2020 Tuning of fly ash loading into chitosan-ethylene glycol diglycidyl ether composite for enhanced removal of reactive red 120 dye: optimization using the Box–Behnken design. *J. Polym. Environ.* **28**, 2720–2733.

Liang, J., Chen, Y., Cai, M., Gan, M. & Zhu, J. 2021 One-pot pyrolysis of metal-embedded biochar derived from invasive plant for efficient Cr(VI) removal. *J. Environ. Chem. Eng.* **9**, 105714.

Lim, J., Lam, K., Bashir, M. J. K. & Yeong, Y. 2016 Spent coffee grounds-based activated carbon preparation for sequestering of malachite green. In *AIP Conference Proceedings 1787*.

Lin, C. S. K., Kaur, G., Li, C., Yang, X. & Stevens, C. V. 2020 *Waste Valorisation: Waste Streams in A Circular Economy, Wiley Series in Renewable Resource*. Wiley, London.

Liu, L., Sun, J., Cai, C., Wang, S., Pei, H. & Zhang, J. 2009 Corn stover pretreatment by inorganic salts and its effects on hemicellulose and cellulose degradation. *Bioresour. Technol.* **100**, 5865–5871.

Liu, Y., Lonappan, L., Brar, S. K. & Yang, S. 2018 Impact of biochar amendment in agricultural soils on the sorption, desorption, and degradation of pesticides: a review. *Sci. Total Environ.* **645**, 60–70.

Liu, J., Zhou, B., Zhang, H., Ma, J., Mu, B. & Zhang, W. 2019 A novel biochar modified by Chitosan-Fe/S for tetracycline adsorption and studies on site energy distribution. *Bioresour. Technol.* **294**, 122152.

Liu, Z., Wang, Z., Chen, H., Cai, T. & Liu, Z. 2021 Hydrochar and pyrochar for sorption of pollutants in wastewater and exhaust gas: a critical review. *Environ. Pollut.* **268**, 115910.

Ma, Y., Qi, Y., Lu, T., Yang, L., Wu, L., Cui, S., Ding, Y. & Zhang, Z. 2021a Highly efficient removal of imidacloprid using potassium hydroxide activated magnetic microporous loofah sponge biochar. *Sci. Total Environ.* **765**, 144253.

Ma, Y., Qi, Y., Yang, L., Wu, L., Li, P., Gao, F., Qi, X. & Zhang, Z. 2021b Adsorptive removal of imidacloprid by potassium hydroxide activated magnetic sugarcane bagasse biochar: adsorption efficiency, mechanism and regeneration. *J. Cleaner Prod.* **292**, 126005.

Mourabet, M., El Rhilassi, A., El Boujaady, H., Bennani-Ziatni, M. & Taitai, A. 2017 Use of response surface methodology for optimization of fluoride adsorption in an aqueous solution by Brushite. *Arab. J. Chem.* **10**, S3292–S3302.

Murthy, P. S. & Naidu, M. M. 2012 Sustainable management of coffee industry by-products and value addition – a review. *Resour. Conserv. Recycl.* **66**, 45–58.

Nguyen, D. L. T., Binh, Q. A., Nguyen, X. C., Huyen Nguyen, T. T., Vo, Q. N., Nguyen, T. D., Phuong Tran, T. C., Hang Nguyen, T. A., Kim, S. Y., Nguyen, T. P., Bae, J., Kim, I. T. & Van Le, Q. 2021 Metal salt-modified biochars derived from agro-waste for effective Congo red dye removal. *Environ. Res.* **200**, 111492.

Nnadozie, E. C. & Ajibade, P. A. 2021 Isotherm, kinetics, thermodynamics studies and effects of carbonization temperature on adsorption of Indigo Carmine (IC) dye using C. odorata biochar. *Chem. Data Collect.* **33**, 100673.

Núñez, J., Yeber, M., Cisternas, N., Thibaut, R., Medina, P. & Carrasco, C. 2019 Application of electrocoagulation for the efficient pollutants removal to reuse the treated wastewater in the dyeing process of the textile industry. *J. Hazard. Mater.* **371**, 705–711.

Pagalan, E., Sebron, M., Gomez, S., Salva, S. J., Ampusta, R., Macarayo, A. J., Joyno, C., Ido, A. & Arazo, R. 2020 Activated carbon from spent coffee grounds as an adsorbent for treatment of water contaminated by aniline yellow dye. *Ind. Crops Prod.* **145**, 1–8.

Peng, X., Hu, F., Zhang, T., Qiu, F. & Dai, H. 2018 Amine-functionalized magnetic bamboo-based activated carbon adsorptive removal of cipro fl oxacin and nor fl oxacin: a batch and fi xed-bed column study. *Bioresour. Technol.* **249**, 924–934.

Rai, A., Mohanty, B. & Bhargava, R. 2016 Supercritical extraction of sunflower oil: a central composite design for extraction variables. *Food Chem.* **192**, 647–659.

Rajesh Banu, J., Kavitha, S., Yukesh Kannah, R., Dinesh Kumar, M., Preethi, M., Atabani, A. E. & Kumar, G. 2020 Biorefinery of spent coffee grounds waste: viable pathway towards circular bioeconomy. *Bioresour. Technol.* **302**, 122821.

Rangabhashiyam, S., Anu, N., Giri Nandagopal, M. S. & Selvaraju, N. 2014 Relevance of isotherm models in biosorption of pollutants by agricultural byproducts. *J. Environ. Chem. Eng.* **2**, 398–414.

Sharifpour, E., Ghaedi, M., Asfaram, A., Farsadrooh, M., Dil, E. A. & Javadian, H. 2020 Modeling and optimization of ultrasound-assisted high performance adsorption of Basic Fuchsin by starch-capped zinc selenide nanoparticles/AC as a novel composite using response surface methodology. *Int. J. Biol. Macromol.* **152**, 913–921.

Shin, J., Bae, S. & Chon, K. 2021 Fenton oxidation of synthetic food dyes by Fe-embedded coffee biochar catalysts prepared at different pyrolysis temperatures: a mechanism study. *Chem. Eng. J.* **421**, 129943.

Sumalinog, D. A. G., Capareda, S. C. & de Luna, M. D. G. 2018 Evaluation of the effectiveness and mechanisms of Acetaminophen and methylene blue dye adsorption on activated biochar derived from municipal solid wastes. *J. Environ. Manage.* **210**, 255–262.

Sun, L., Tian, C., Li, M., Meng, X., Wang, L., Wang, R., Yin, J. & Fu, H. 2013 From coconut shell to porous graphene-like nanosheets for high-power supercapacitors. *J. Mater. Chem. A* **1**, 6462–6470.

Theydan, S. K. & Ahmed, M. J. 2012 Adsorption of methylene blue onto biomass-based activated carbon by FeCl3 activation: equilibrium, kinetics, and thermodynamic studies. *J. Anal. Appl. Pyrolysis* **97**, 116–122.

Tomin, O., Vahala, R. & Roza, M. 2021 Tailoring metal-impregnated biochars for selective removal of natural organic matter and dissolved phosphorus from the aqueous phase. *Microporous Mesoporous Mater.* **328**, 111499.

Topare, N. S. & Bokil, S. A. 2020 Adsorption of textile industry effluent in a fixed bed column using activated carbon prepared from agro-waste materials. *Mater. Today Proc* **43**, 530–534.

Tran, H. N., You, S. J. & Chao, H. P. 2016 Effect of pyrolysis temperatures and times on the adsorption of cadmium onto orange peel derived biochar. *Waste Manag. Res.* **34**, 129–138.

Tripathi, M., Sahu, J. N. & Ganesan, P. 2016 Effect of process parameters on production of biochar from biomass waste through pyrolysis: a review. *Renewable Sustainable Energy Rev.*. **55**, 467–481.

Vardon, D. R., Moser, B. R., Zheng, W., Witkin, K., Evangelista, R. L., Strathmann, T. J., Rajagopalan, K. & Sharma, B. K. 2013 Complete utilization of spent coffee grounds to produce biodiesel, bio-oil, and biochar. *ACS Sustain. Chem. Eng.* **1**, 1286–1294.

Wen, X., Liu, H., Zhang, L., Zhang, J., Fu, C., Shi, X., Chen, X., Mijowska, E., Chen, M. J. & Wang, D. Y. 2019 Large-scale converting waste coffee grounds into functional carbon materials as high-efficient adsorbent for organic dyes. *Bioresour. Technol.* **272**, 92–98.

Wirawan, T., Koesnarpadi, S. & Widodo, T.-N. 2020 Study of Rhodamine B adsorption onto activated carbon from spent coffee grounds. In *AIP Conference Proceedings 2237*.

Xiao, X., Chen, B., Chen, Z., Zhu, L. & Schnoor, J. L. 2018 Insight into multiple and multilevel structures of biochars and their potential environmental applications: a critical review. *Environ. Sci. Technol.* **52**, 5005–5518.

Yao, X., Ji, L., Guo, J., Ge, S., Lu, W., Chen, Y., Cai, L., Wang, Y. & Song, W. 2020 An abundant porous biochar material derived from wakame (Undaria pinnatifida) with high adsorption performance for three organic dyes. *Bioresour. Technol.*, 318, 124082.

Yu, K. L., Lee, X. J., Ong, H. C., Chen, W. H., Chang, J. S., Lin, C. S., Show, P. L. & Ling, T. C. 2021 Adsorptive removal of cationic methylene blue and anionic Congo red dyes using wet-torrefied microalgal biochar: equilibrium, kinetic and mechanism modeling. *Environ. Pollut.* **272**, 115986.

Zeng, S. & Kan, E. 2021 Adsorption and regeneration on iron-activated biochar for removal of microcystin-LR. *Chemosphere* **273**, 129649.

Zhang, F., Chen, X., Wu, F. & Ji, Y. 2016 High adsorption capability and selectivity of ZnO nanoparticles for dye removal. *Colloids Surfaces A Physicochem. Eng. Asp.* **509**, 474–483.

First received 27 January 2022; accepted in revised form 5 April 2022. Available online 18 April 2022